A 3-D printed E-plane waveguide magic-T using air-filled coax-to-waveguide transitions

Guo, Cheng; Li, Jin; Yu, Yang; Zhang, Fan; Zhu, Yujian; Yang, Qian; Zhu, Weijun; Zhu, Shitao; Shang, Xiaobang; Gao, Yang; Wang, Yi; Huang, Guan-long; Cheng, Qingsha S.; Zhang, Anxue

DOI:
10.1109/TMTT.2019.2944355

License:
Other (please specify with Rights Statement)

Document Version
Peer reviewed version

Citation for published version (Harvard):
Guo, C, Li, J, Yu, Y, Zhang, F, Zhu, Y, Yang, Q, Zhu, W, Zhu, S, Shang, X, Gao, Y, Wang, Y, Huang, G, Cheng, QS & Zhang, A 2019, 'A 3-D printed *E*-plane waveguide magic-T using air-filled coax-to-waveguide transitions', *IEEE Transactions on Microwave Theory and Techniques*, vol. 67, no. 12, pp. 4984-4994. https://doi.org/10.1109/TMTT.2019.2944355

A 3-D Printed *E*-Plane Waveguide Magic-T Using Air-Filled Coax-to-Waveguide Transitions

Cheng Guo, Jin Li, Yang Yu, Fan Zhang, Yujian Zhu, Qian Yang, Weijun Zhu, Shitao Zhu Xiaobang Shang, *Senior Member*, *IEEE*, Yang Gao, Yi Wang, *Senior Member*, *IEEE* , Guan-Long Huang, *Senior Member*, *IEEE*, Qingsha S.Cheng, *Senior Member*, *IEEE* , and Anxue Zhang

***Abstract*—This paper reports on a new class of broadband and fully 3-D printed *E*-plane coax-to-waveguide transition and a monolithically 3-D printed waveguide magic-T based on the transition. The transition is constructed by a section of air-filled rectangular coaxial transmission line that is placed between two broadband coax-to-waveguide probe transitions. It is used to interconnect the magic-T's sum port and the waveguide T-junction. The incorporation of the transition reorients all the waveguide arms of the magic-T into the *E* plane. Some *X*-band prototypes of the proposed transition and magic-T are designed and implemented. Polymer-based additive manufacturing and copper electroplating techniques are employed to fabricate each prototype monolithically. The transition as well as the magic-T exhibits broadband and low-loss characteristics from 8.2 to 12.4 GHz with measured performance well matched with the simulations. Additionally, the power handling capability (PHC) including the peak PHC (PPHC) and the average PHC (APHC) of the magic-T is evaluated by simulations, showing that the proposed magic-T could handle 100 W of APHC.**

***Index Terms*—Additive manufacturing, air-filled coaxial transmission line, coax-to-waveguide transition, *E*-plane waveguide magic-T, stereolithography apparatus.**

Manuscript received May 3, 2019. revised Aug 21, accepted Sept 8. This work was supported in part by the NSFC fund under Grants No. 61801300, 61701367,61601323, in part by the Fundamental Research Funds for the Central Universities under Grant xxj032019001, in part by the New Teacher Natural Science Research Project of Shenzhen University under Grant No. 2018078. This paper is an expanded version from the IEEE MTT-S International Microwave Symposium (IMS2019), Boston, MA, USA, June 2–7, 2019. (*Corresponding authors: Cheng Guo and Anxue Zhang*.)

C. Guo, Q. Yang, S.Zhu and A. Zhang are with the Department of Inf and Communication Engineering, Xi'an Jiaotong University, Xi'an, Shaanxi 710049, China. C. Guo is also with Department of Electronic, Electrical and Systems Engineering, University of Birmingham, Edgbaston, Birmingham, B15 2TT, U.K. (email: spmguo@163.com; anxue.zhang@xjtu.edu.cn).

J. Li, Y. Zhu, G.-L. Huang are with the Guangdong Provincial Mobile Terminal Microwave and Millimeter-Wave Antenna Engineering Research Center, College of Electronics and Information Engineering, Shenzhen University, Shenzhen, Guangdong 518060, China.

Y. Yu and Q. S. Cheng are with the Department of Electrical and Electronic Engineering, Southern University of Science and Technology, Shenzhen, Guangdong 518055, China.

F. Zhang is with the School of Physics, University of Electronic Science and Technology of China, Chengdu, Sichuan 610054, China.

W.Zhu is with School of Mechanical Engineering and Automation, Beihang University, Beijing, 100010,China.

Y.Gao is with School of Information Engineering, Zhengzhou University, Zhengzhou, 450000,China

Y. Wang is with the Department of Electronic, Electrical and Systems Engineering, University of Birmingham, Edgbaston, Birmingham B15 2TT, U.K..

X. Shang is with the National Physical Laboratory, Teddington, Middlesex TW11 0LW, U.K..

C. Guo and J. Li contributed equally to this paper.

I. Introduction

As one of fundamental passive components in microwave front-end communication systems, low-loss, broadband, size-compact, and easily integrated transitions have been in high demand to interconnect different types of transmission lines (TLs) and various port structures of devices. Several high-performance TL transitions (e.g., [1]–[3]) have been reported as conjunctions among rectangular waveguides, coaxial cables, and planar TLs such as microstrip lines and coplanar waveguides (CPWs). For instance, commercially available waveguide-to-coax adapters have been widely used for microwave measurement. Microstrip-to-waveguide [1], [2] and CPW-to-waveguide [3] transitions have been essential parts in the package of hybrid integrated microwave circuits. Conventionally, these types of transitions are practically implemented by exciting a rectangular waveguide with an in-line or vertically placed *E*-plane probe, enabling the transformation of the propagation modes and a broadband matching of characteristic impedances between these two types of TLs. These TL transitions can be applied to construct many multiport waveguide components such as power dividers/combiners (e.g., [4]) and magic-Ts (e.g., [5]), showing enhanced design flexibility. However, integrating such probe transitions into metallic waveguides can be labor-intensive, because most conventional TL transitions are implemented by employing subtractive manufacturing and printed-circuit-board (PCB) technologies, where split-block computer numerical controlled (CNC) milling and precise assembly of multiple manufactured parts are involved.

Magic-Ts are common four-port power dividing/combining networks that support in-phase and out-of-phase transmissions of the output signals and meanwhile offer isolations between the sum and difference inputs. They can be physically constructed using various TL architectures such as metallic waveguides [5]–[7], substrate integrated waveguides [8]–[13], and substrate integrated suspended lines [14]. Correspondingly, many fabrication techniques such as metal-based CNC milling [5]–[7], single/multi-layer PCB process [8]–[11], [14] and low-temperature co-fired ceramic technology [12], [13] have been developed to implement the magic-Ts. Waveguide magic-Ts exhibit better power handling capability than the planar counterparts, while they suffer from bulky and incompact packages because of different orientations of the waveguide arms. Coplanar waveguide arms can be designed to reorient all the waveguide ports in the same plane, facilitating

microwave measurement and simplifying assembly of the RF systems [5]–[7]. In these scenarios, broadband transitions between the T-junction and the other waveguide port of the magic-T are required. For example, a microstrip probe transition can be used in the *E*-plane magic-T [5]. Unfortunately, the power handling capability of the magic-T is weakened due to limitation in the power handling capability of the microstrip line. A solution to address this issue can be interconnecting the T-junction and the other waveguide port of the magic-T with a ridged waveguide probe transition [6], [7]. However, this results in geometrically complex impedance matching structures and increases difficulties in the fabrication and assembly. To manufacture the ridged waveguide probe, the magic-T has to be split into multiple parts for milling individually. This requires precise alignment and assembly of the milled parts [5].

In this work, a solution for the design and monolithic implementation of an *E*-plane waveguide magic-T is provided. The magic-T is based on the authors' IMS2019 conference paper [15], where a broadband *E*-plane coax-to-waveguide transition based on air-filled self-suspended rectangular coaxial TL is demonstrated with good RF performance. In addition to attractive merits of the TL such as little dispersion and negligible dielectric and radiation losses, the paper also highlights the fabrication scheme of the entire transition using polymer-based additive manufacturing (also known as 3-D printing). In [15], the design, fabrication, and measurement of the transition have been described, and it is mentioned that the transition can be used to build functional waveguide components. However, practical applications of the transition have not been presented in the conference paper.

Therefore, aiming to validate the usefulness of the transition in typical functional waveguide components, this work focuses on the design and realization of an *E*-plane waveguide magic-T composed of the transition. The transition is used as an alternative for either a microstrip probe or a ridged waveguide probe to interconnect the T-junction and the other waveguide ports of the magic-T. It is designed to be practically integrated with other structures of the magic-T into a single part. It should be mentioned that many other applications of the transition such as couplers and power dividers/combiners are possible, and therefore, the limited number of demonstration of this paper does not degrade the novelty of the transition in [15]. In addition, the magic-T is fabricated monolithically by incorporating polymer-based stereolithography apparatus (SLA) and copper electroplating. The proposed magic-T features potentially enhanced power handling capability as compared to the one composed of microstrip probes [6]. The power handling capability of the magic-T is evaluated by the result from electromagnetic (EM)-thermal co-simulation. The related analysis is not discussed in the authors' previous work.

The following content of this paper is organized as follows. The RF design of the proposed *X*-band waveguide magic-T is presented in Section II. The broadband air-filled rectangular-coax-to-waveguide transition proposed in [15] is again highlighted in this Section, because it is the most important part of the magic-T and it also shows great potential in many other applications such as power combiners [16], wideband filters [17], and couplers [18]. The fabrication process of the *X*-band transition and magic-T prototypes is introduced in Section III. The microwave measurement of the transition and the magic-T is described in Section IV. The power handling capability of the magic-T is analyzed in Section V.

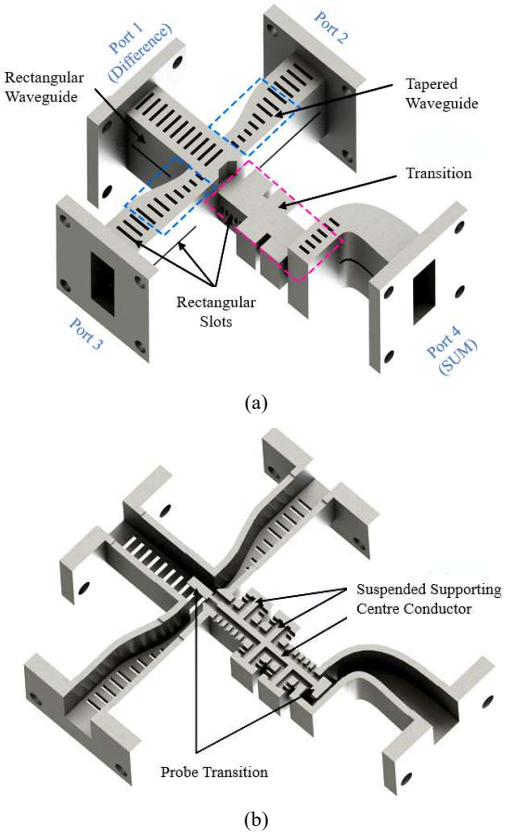

Fig. 1. Structural illustrations of the proposed monolithically integrated *E*-plane waveguide magic-T using air-filled rectangular-coax-to-waveguide transitions. (a) The complete fabrication model. (b) The *E*-plane profile showing the internal geometry.

II. Design of the *X*-Band Coax-to-Waveguide Transition and the *E*-Plane Waveguide Magic-T

The proposed *E*-plane waveguide magic-T is illustrated in Fig. 1. It is comprised of a conventional waveguide T-junction power divider involving the waveguide ports 1–3 and a broadband air-filled coaxial TL-based transition from the port 4 to the T-junction.

The transition consists of a segment of air-filled self-suspended rectangular coaxial TL. The center conductor of the coaxial TL is placed at the *E* plane of the waveguides and each of its terminals is shaped as a rectangular probe. One of the probes is inserted into the waveguide T-junction from the symmetrical center. The other one is inserted along the *E*-plane center of a reduced-height waveguide that is tapered from the waveguide port 4. These two probes effectively couple RF power from the waveguides to the coaxial TL. Particularly, the waveguide connecting to port 4 is bent in 90° to facilitate the measurement. For the T-junction, tapered and reduced-height waveguides are used for the waveguide arms connecting to the

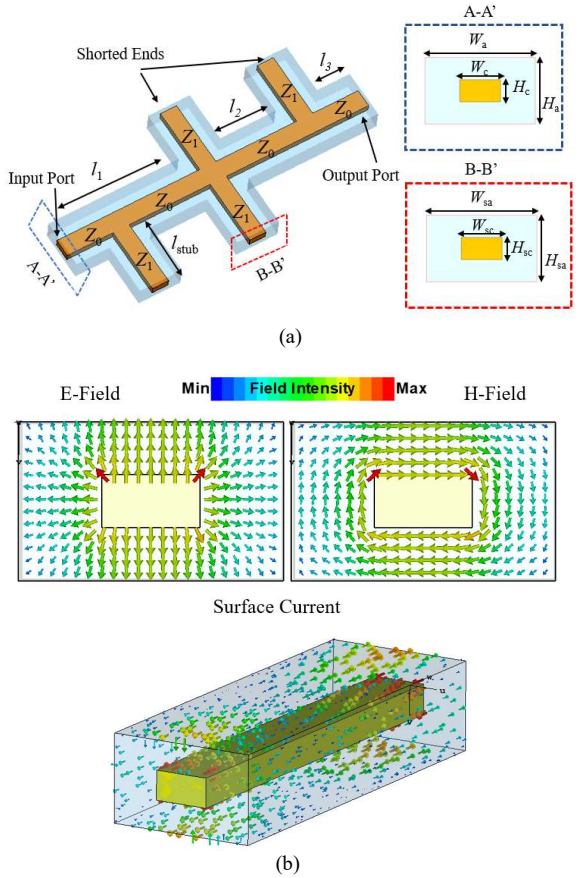

Fig. 2. The designed 50-Ω air-filled self-supported rectangular coaxial TL. (a) The 3-D air-box simulation model, where Z_0 = 50 Ω and Z_1 = 52.5 Ω. (b) The port EM field distribution and the surface current.

TABLE I
CRITICAL DIMENSIONS OF THE RECTANGULAR COAXIAL TL (UNITS: MM)

l_1	l_2	l_3	l_{stub}	W_c	H_c	W_{sc}	H_{sc}	W_a	H_a	W_{sa}	H_{sa}
15.252	8.665	4.869	6.945	1.85	1	1.718	1	5	3	4.439	3

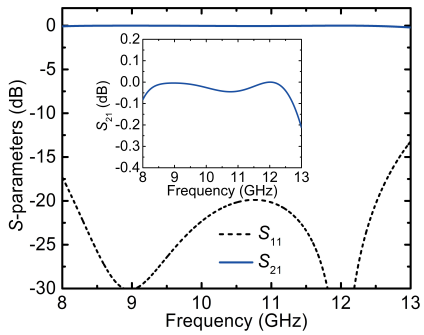

Fig. 3. EM-simulated *S*-parameters of the designed *X*-band air-filled rectangular coaxial TL. The electrical conductivity of 5.96 × 10^7 S/m was used for copper boundaries.

ports 2 and 3, while a straight rectangular waveguide is used for the arm connecting to the port 1, as labeled in Fig. 1.

The working principle of the proposed magic-T is summarized as follows—1) if an RF signal is input from the port 1, it propagates to the ports 2 and 3 like a conventional T-junction, whereas the port 4 is isolated because the electric field of the port 1 is perpendicular to the probe orientation at the T-junction; 2) if the RF signal is input from the port 4, it is output at the ports 2 and 3 via the transition, and the port 1 is isolated, because the electric fields at port 2 and 3 are in parallel with the probe orientation whereas it is not the case at the port 1; 3) in either aforementioned case, the output ports 2 and 3 ideally share the power equally, and the output signals are out of phase for the first case whereas in phase for the second case. Therefore, the ports 1 and 4 are the difference and sum ports, respectively. The RF design of the waveguide T-junction power divider can be found in [19] and is not repeated in this paper. The following content describes progressively RF designs of the air-filled self-suspended rectangular coaxial TL, the coax-to-waveguide transition, and the magic-T.

A. Air-Filled Self-Suspended Rectangular Coaxial TLs

Fig. 2(a) shows the air-filled self-supported rectangular coaxial TL. The TL is comprised of a rectangular inner conductor that is located symmetrically inside a concentric rectangular hollow outer conductor. It is structurally supported by four rectangular, quarter-wavelength, and end-shorted stubs that are placed at appropriate intervals along the propagation direction of the TL. These stubs are equivalently open-circuited at the point connecting to the inner conductor, and therefore the propagated signal is not affected. It needs to be noticed that if only one stub is used to support the TL, the bandwidth can be very narrow but for this particular case, the three stubs work together and the bandwidth can be enhanced to more than 47.5%, as detailed in the wideband filter design in [18]. The conductor and the supporting stubs have characteristic impedances of Z_0 and Z_1, respectively. In order to simply the design, the four stubs are designed to have the same length l_{stub} as labeled in Fig. 2(a) and the same characteristic impedance. Such a TL supports propagation of a TEM mode, and this is verified by the EM field distribution illustrated in Fig. 2(b). The EM field and surface current obtained by performing EM simulation in the Computer Simulation Technology (CST) Studio Suite shows a strong similarity to that of a circular coaxial TL.

In this design, the cross-section dimensions of the TL were selected to exhibit a 50-Ω characteristic impedance for the TL at the center frequency, i.e., 10 GHz, of *X* band. First, 1-mm thicknesses H_c and H_{sc} for all inner conductors and 5 mm × 3 mm profiles for all outer conductors were initialized taking into consideration of the design simplification, manufacturability, and practical mechanical strength. The widths W_c and W_{sc} of the inner conductor, as labeled in Fig. 2(a), can be determined by using the equations in [17] for a 50-Ω characteristic impedance. Note that Z_1 and Z_0 were initially designed to be 50 Ω, but to compensate the junction effect, the characteristic impedance Z_1 for the supporting stubs was optimized to be 52.5 Ω. The finalized dimensions of the TL are included in Table I. Fig.3 shows the frequency responses of the designed *X*-band TL. From 8 to 13 GHz, the EM-simulated insertion and return losses (IL and RL) are less than 0.1 dB and better than 20 dB, respectively, showing a broadband and low-loss transmission characteristic, as shown in Fig.3. Further simulated result shows that with the designed physical dimensions the

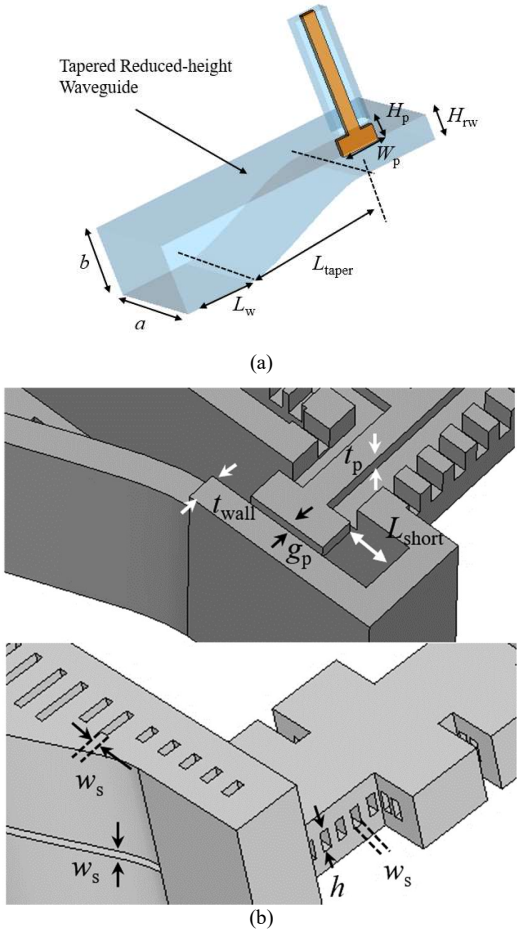

Fig. 4. Structural illustrations of the proposed rectangular-coax-to-waveguide probe transition. (a) The air-box simulation model. (b) The *E*-plane profile (up) and the external package (down) of the probe transition.

TABLE II
CRITICAL DIMENSIONS OF THE RECTANGULAR-COAX-TO-WAVEGUIDE PROBE TRANSITION (UNITS: MM)

a	b	L_w	L_{taper}	L_{rw}	H_{rw}	W_p	H_p	t_p	g_p	h	L_{short}	t_{wall}	w_s
22.86	10.16	10	20.13	11.9	3.79	5.52	2.45	1	0.44	2.5	3.76	2	1

rectangular coaxial TL (excluding the end-shorted supporting stubs) can operate under a single TEM mode up to 28.4 GHz, and beyond this frequency the first higher order mode of the TL appears.

Previously, such a TL architecture could be manufactured by employing micromachining process based on either SU-8 photoresist thick films or deep reactive ion etch, as exemplified in [17]–[18] and [20]–[22]. The engineered devices usually consist of multiple layers that need to be carefully aligned and assembled. The related technologies have been applied to micromachined bandpass filters, antennas, and couplers operating from *K* to terahertz band [21].

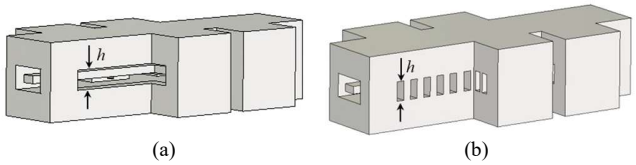

Fig.5. Two possible slots for the coaxial TL. (a) A single slot parallel to the current. (b) A slot array with equal height with the single slot.

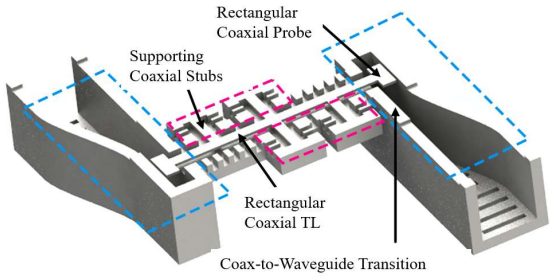

Fig. 6. Structural illustrations of the designed transitions in a back-to-back configuration.

B. Air-Filled Rectangular-Coax-to-Waveguide Transitions

A package designed for the probe transition is illustrated in Fig. 4(b). It should be noticed that many rectangular through slots with identical width w_s are designed on the sidewalls of the waveguide. These slots are designed to facilitate the fabrication and the electroplating of the structure, and this will be further discussed in Section III. These slots are ideally non-radiative as they are specially designed. 1) For the rectangular waveguide, such slots are in parallel with the surface current of the TE_{10} mode, hence little radiation can be generated, this is similar to the case discussed in [23]-[24]. 2) For the slots on the coaxial TL, it appears to be counterintuitive that little radiation will be generated as the slots are in perpendicular with the surface current of the TEM mode (as shown in Fig.2(b)). To understand this, consider the model shown in Fig.5(a), where a single slot with a height of 2.5 mm was opened on the sidewalls on the coaxial TL and apparently this slot orientation is in parallel with the current. EM simulation shows insertion and return losses about 0.1 dB and better than 20 dB across the *X*-band, respectively. Additionally, the simulated total radiation efficiency for this structure is about -48 dB, showing that little radiation was generated by this slot. 3) In Fig.4 and Fig.5 (b), we have added an array of supports along the single slot, not only to make the coaxial structure mechanically stronger but also made it self-supported during the 3D printing process, this will be detailed in section III. EM simulations show little difference between the structures in Fig.5(a) and Fig.5(b), in terms of insertion/return loss as well as the radiation. In future works, electroless plating [27] can be used to replace the electroplating process used in this paper to avoid the use of these slots, hence no radiation will be generated. Finally, the detailed design parameters for the transition are included in Table II.

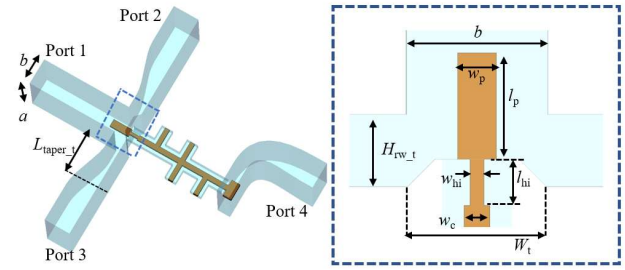

Fig. 7. Structural details for the T-junction of the designed *X*-band waveguide magic-T.

TABLE III
CRITICAL DIMENSIONS OF THE WAVEGUIDE T-JUNCTION (UNITS: MM)

a	b	H_{rw_t}	L_{taper_t}	w_p	w_{hi}	W_t	H_t	l_p	l_{hi}
22.86	10.16	5.197	20	2.787	1.011	10	1.982	7.631	3.314

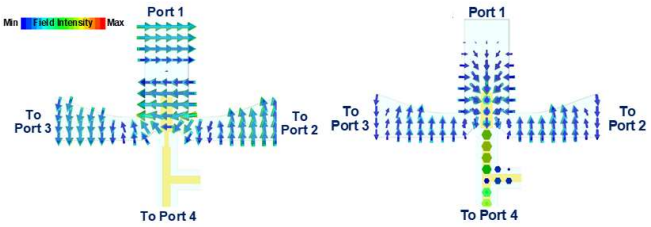

(a) (b)

Fig. 8. Electric field distribution in the waveguide magic-T: (a) The in-phase transmission (input from the port 4). (b) The out of-phase transmission (input from the port 1).

In order to experimentally validate RF performance of the proposed transition, a device including a pair of the transitions in a back-to-back configuration connected with the air-filled rectangular coaxial TL in between is designed and shown in Fig. 6. To avoid repetition, the simulated results will be compared with the measured result in the next Section.

C. Waveguide Magic-T

As is shown in Fig. 1, the proposed waveguide magic-T is built by connecting the rectangular-coaxial-to-waveguide transition to the waveguide T-junction. The end of the TL inserting into the T-junction is shaped as a rectangular probe and is placed along the symmetrical line of the *E* plane of the T-junction. Under such circumstance, good isolation between the ports 1 and 4 and the minimum amplitude and phase imbalances between the ports 2 and 3 can be obtained. A short segment of high-impedance TL that behaves as an inductive impedance transformer is used to interconnect the probe and the main TL. Other structures at the T-junctions designed for a broadband impedance matching include a corner cut (with a length W_t and a height H_t as labeled in Fig. 7) and tapered height-reduced waveguides (in a length L_{taper_t}) to the ports 2 and 3. The rest critical dimensions of the magi-T are included in Table III, and the other design parameters are mostly the same to the ones in Tables I and II. Optimization of these design parameters was performed in CST. Note that some of the dimensions were slightly adjusted after the slotted package was added.

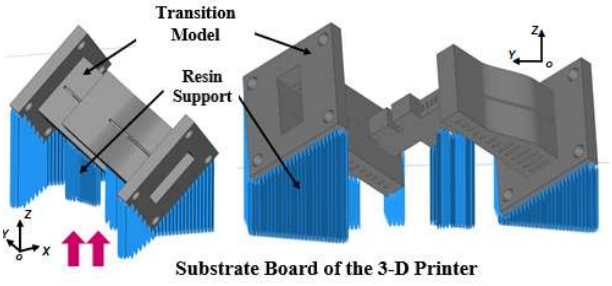

(a)

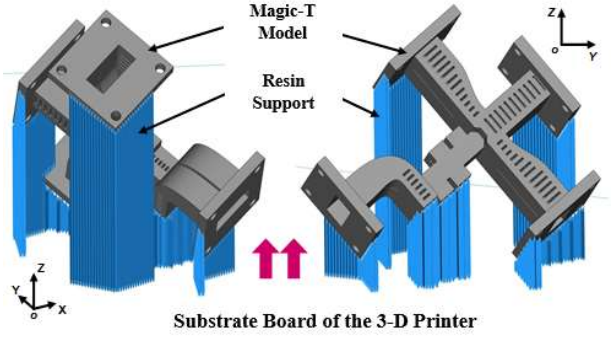

(b)

Fig. 9. Illustrations of the tilted 3-D printing postures. (a) For the waveguide-coax-waveguide transition. (b) For the waveguide magic-T.

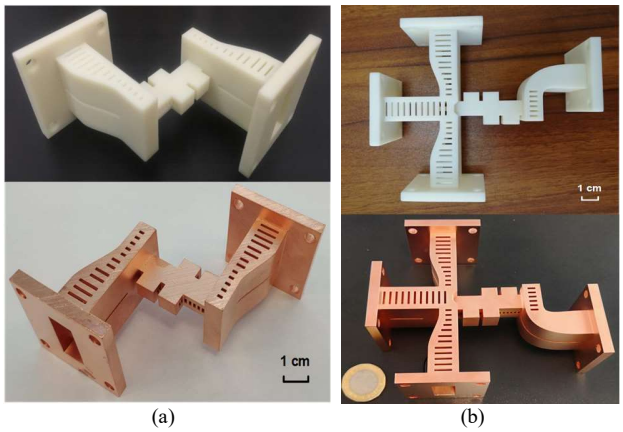

(a) (b)

Fig. 10. Photographs of the SLA-printed prototypes before and after surface metallization. (a) The waveguide-coax-waveguide transition. (b) The magic-T.

Again, in order to clearly present the working principle of the proposed magic-T, the electric field distribution inside the magic-T is illustrated in Fig. 8 for in-phase and out-of-phase transmissions. For the in-phase transmission, i.e., input from the port 4, as shown in Fig. 8(a), the RF power is divided equally in magnitude to the ports 2 and 3 with the same phase, and it is not coupled to the port 1. For the out-of-phase transmission, i.e., input from the port 1, as shown in Fig. 8(b), the RF power is also divided equally in magnitude to the ports 2 and 3, but with a 180° phase difference indicated by the opposite directions of the output electric field.

The EM-simulated result of the magic-T shows at full *X* band a 3-dB power dividing performance with simulated amplitude

and phase imbalances close to zero and good 1-to-4 and 2-to-3 port isolations of >80 dB and >20 dB, respectively. The simulated port return losses are all greater than 16 dB. The simulated and measured results will be presented in Section IV.

III. Device Fabrication

The *X*-band prototypes of the proposed transition and waveguide magic-T were 3-D printed by using SLA and copper electroplating techniques. Similar fabrication approach has been reported in the additive manufacturing of microwave waveguide filters [23]–[25]. Before the 3-D printing process was carried out, structural compensation was performed to the electronic model of the transition and the magic-T. In the structural compensation, the thickness of the copper layer to be plated was subtracted from the model. This is to minimize the dimensional tolerance induced by the plated copper layer. Then, each printing model was placed in a properly tilted posture for SLA printing to make sure as little supporting material as possible would be required inside. An exemplified tilted posture for each model is shown in Fig. 9. Under such printing postures, a very small amount of internal linear support appeared at the head of each rectangular probes, and the support could be removed during the post process. The devices were SLA-printed in a vertical resolution of 70 μm with a ceramic-filled photosensitive resin Somos PerForm.

The polymer-based additive manufacturing of the devices in this work has the following advantages. 1) Splitting a complex structure into multiple parts for fabrication is no longer required, and time-consuming and labor-intensive assembly can be avoided, which significantly improves the fabrication efficiency. 2) The assembly tolerance can be eliminated. 3) Little support material is needed internally as the printing postures are specially designed to make sure the structure to be self-supported. 4) The redundant structural material has been removed and the weight of the device can be highly reduced.

In the metallization process, a 10-μm thick conductive layer of copper was electroplated onto the resin on a seed layer of electroless plated nickel. Note that this thickness of 10 μm is over 10× the skin depth of copper (0.729 μm calculated at 8 GHz). For the magic-T, the copper layer was further thickened to at least 30 μm to enhance the thermal handling capability for the magic-T. Photographs of the fabricated prototypes are included in Fig. 10.

IV. Measurement and Discussion

The transition was measured by using a Keysight E8362C network analyzer under a two-port waveguide thru-reflect- line calibration. The simulated and measured results are graphically compared in Figs. 11(a)–(c), showing good agreement. The transition exhibits a measured RL of mostly better than 15 dB, and a corresponding average IL of 0.5 dB in the *X* band. The loss, defined as $1 - |S_{11}|^2 - |S_{21}|^2$, of the transition calculated from the measured *S* parameters is in the range of 0.2−0.6 dB. The increment of 0.1−0.5 dB in the IL is mainly attributed to the degraded electrical conductivity of the plated copper due to surface roughness and surface oxidation that they were not

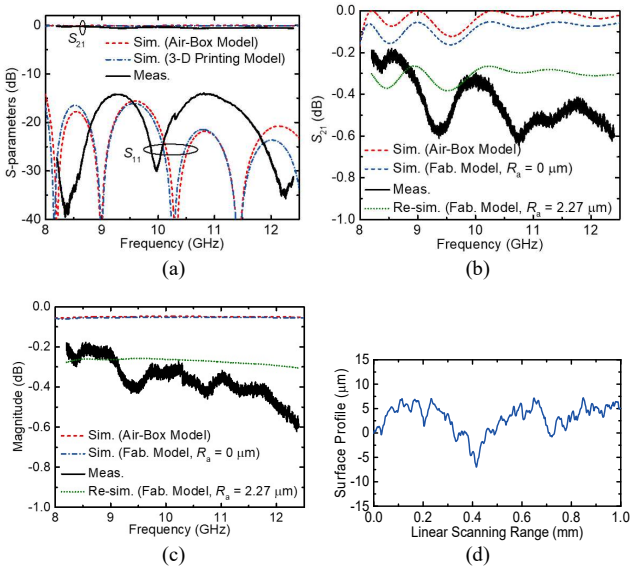

Fig. 11. The designed *X*-band back-to-back rectangular-coax-to-waveguide transition. (a) EM-simulated and RF-measured S_{11} and S_{21} parameters. (b) A zoom-in view of the S_{21} parameter. (c) The loss $(1 - |S_{11}|^2 - |S_{21}|^2)$ of the transition. (d) A measured surface profile in the waveguide flange region of the fabricated transition.

taken into consideration in the simulation. In order to quantify the surface roughness, the surface profile in an arbitrarily selected region of the waveguide flange of the fabricated transition was measured by utilizing a Bruker Dektak-XT stylus profiler. A linear scan was performed in a length of 1000 μm under a sampling resolution of 0.333 μm. A typical measured surface profile is plotted in Fig. 12(d). In the entire scanning range, the measured surface profile has peak and valley values of surface roughness of around ±7 μm. The measured average surface roughness (R_a) and root mean square surface roughness (R_q) values are 2.271 and 2.846 μm, respectively. Taking into account the measured roughness value, the IL of the transition would be increased to 0.26−0.38 dB, and the loss $(1 - |S_{11}|^2 - |S_{21}|^2)$ of the transition would be increased to around 0.3 dB. The corresponding re-simulated RF performance taking the roughness value into consideration is included in Figs. 11(b) and 11(c) for comparison. It should be mentioned that the internal surface of the transition might suffer larger roughness since it was not polished as well as the outside.

When the waveguide magic-T was measured using the two-port network analyzer, the rest two unused ports were connected to *X*-band waveguide matching loads. The results are compared in Fig. 12. In Figs. 12(a) and 12(b), the measured port RLs are greater than 17 dB in the entire *X* band for the port 1–3 and better than 12 dB for the port 4. In Figs. 12(c) and 12(d), the measured transmission coefficients for the output arms are in the range of -3.8–-3.4 dB for the in-phase transmission, and -3.5–-3.2 dB for the out-of-phase transmission. The corresponding transmission losses are 0.3–0.5 dB higher than the simulated values. In Figs. 12(e) and 12(f), the measured amplitude imbalances are -0.4–0.2 dB for the in-phase transmission, and -0.5–0 dB for the out-of-phase transmission. The measured phase imbalances are (-3–3)° for the in-phase

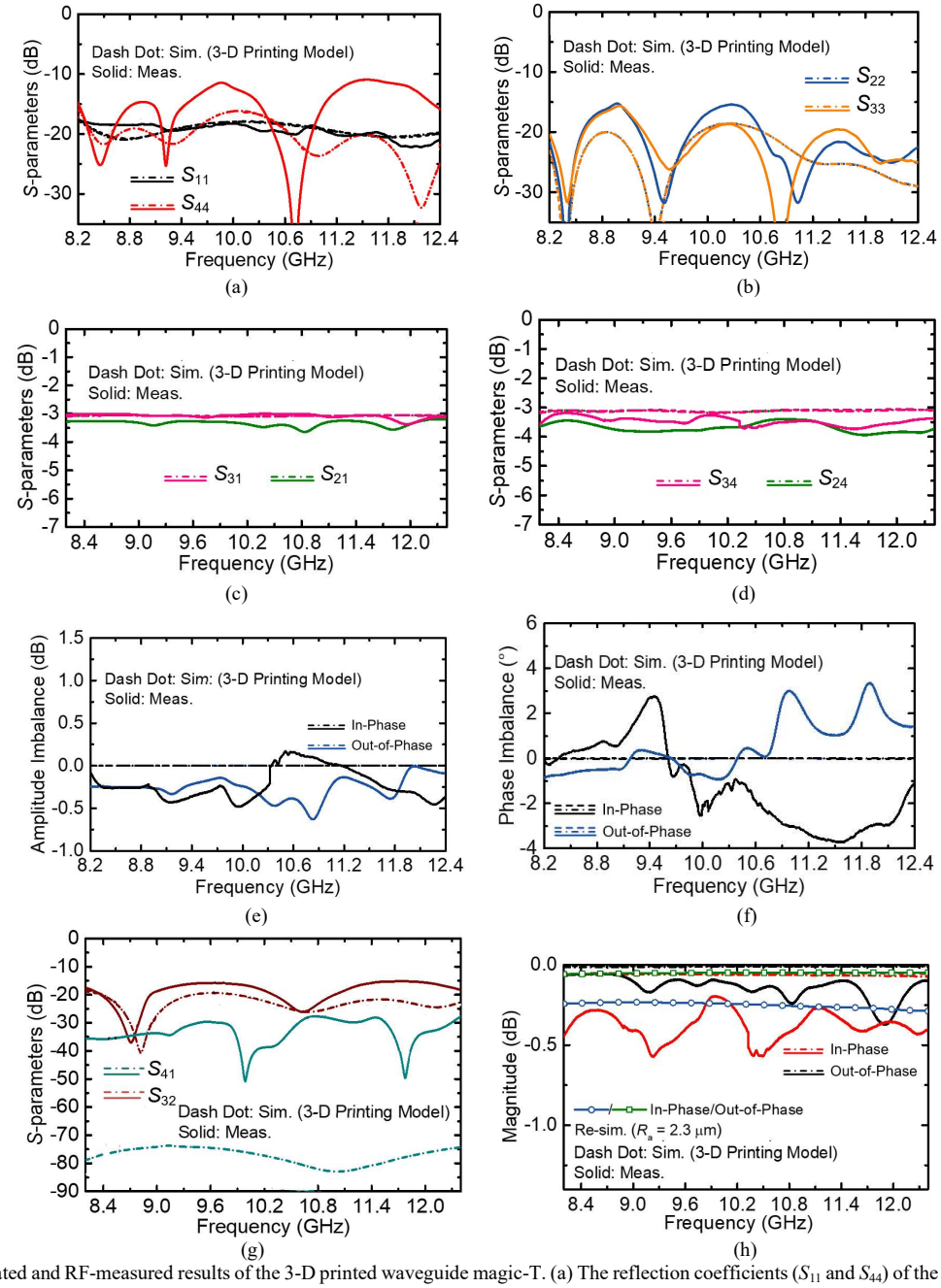

Fig. 12. EM-simulated and RF-measured results of the 3-D printed waveguide magic-T. (a) The reflection coefficients (S_{11} and S_{44}) of the ports 1 and 4. (b) The reflection coefficients (S_{22} and S_{33}) of the ports 2 and 3. (c) The out-of-phase transmission coefficients (S_{31} and S_{21}). (d) The in-phase transmission coefficients (S_{34} and S_{24}). (e) The amplitude imbalance. (f) The phase imbalance. (g) The port isolations. (h) The calculated losses (1 - $|S_{14}|^2$ - $|S_{24}|^2$ - $|S_{34}|^2$ - $|S_{44}|^2$) and (1 - $|S_{11}|^2$ - $|S_{21}|^2$ - $|S_{31}|^2$ - $|S_{41}|^2$) for the in-phase and out-of-phase transmissions, respectively.

transmission, and (-1–3)° for the out-of-phase transmission. As shown in Fig. 12 (g), the measured 2-to-3 port isolation is higher than 16 dB, whereas the measured 1-to-4 port isolation is degraded to around 30 dB. This is attributed to slight deformation of the coaxial probe deviating from the symmetrical line as a result of residual stress and creep of the cured resin.

Finally, the conductor losses (1 - $|S_{14}|^2$ - $|S_{24}|^2$ - $|S_{34}|^2$ - $|S_{44}|^2$) and (1 - $|S_{11}|^2$ - $|S_{21}|^2$ - $|S_{31}|^2$ - $|S_{41}|^2$) for the in-phase and out-of-phase transmissions, respectively, are calculated and plotted in Fig. 12(h). The practical loss for the in-phase transmission is 0.2–0.5 dB, and for the out-of-phase transmission is 0.1–0.3 dB. The small losses indicate good quality in the plated copper layer and negligible radiation loss from the slots. These loss values are also critical to the calculation of the power handling capability because the conductor losses are actually converted into heat.

V. Power Handling Capability of the Magic-T

The power handling capability (PHC) including the peak PHC (PPHC) and the average PHC (APHC) of the magic-T is

TABLE IV
COMPARISON WITH PREVIOUSLY REPORTED *E*-PLANE WAVEGUIDE MAGIC-T

Ref.	*f* (GHz)/(RBW)	LOP (dB)	LIP (dB)	Isolation (dB)	A.I. (dB)	P.I. (°)	Transition Structures	Fabrication Techniques	Number of Parts	[a]APHC (W)
[5]	27.5–34/(21.1%)	<0.15	<0.35	>20	0.25	<2	Microstrip probe	CNC + PCB	3	17
[6]	7.8–9.4/(18%)	<0.2	<0.5	>26	0.1	<1	Ridged waveguide	CNC	3	N/A
[7]	28–36/(25%)	<0.15	<1	>21	0.2	<7	Ridged waveguide	CNC	2	240
T.W.	8.2–12.4/(42%)	<0.5	<0.8	>16	<0.5	<3	Air-filled coaxial TL	3-D printing	1	100

[*]T.W.: This work; *f*: The operational frequencies; RBW: The relative bandwidth with reference to the mid-band frequency; LOP and LIP: The transmission losses for the out-of-phase and in-phase transmissions, respectively; A.I.: Amplitude imbalance; P.I.: Phase imbalance; N/A: Not available.

[a]The APHC was evaluated using the simulated values.

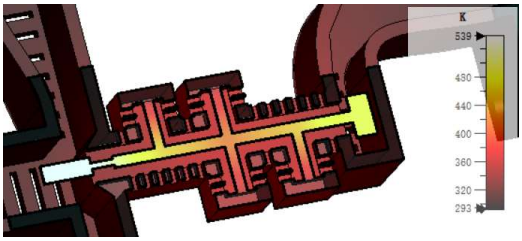

(a)

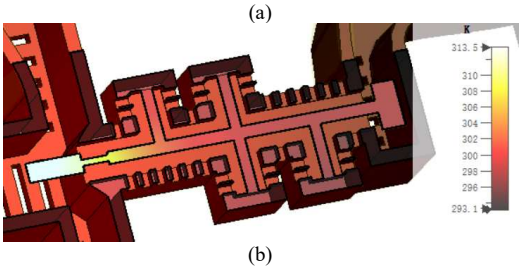

(b)

Fig. 13. The simulated temperature distribution of the magic-T under 100-W input power. (a) From the in-phase port. (b) From the out-of-phase port.

evaluated in this Section.

A. PPHC

The PPHC of the magic-T is limited by the electric field strength threshold for the air breakdown, i.e., 3 kV/mm [7]. As the input power in CST is set the default as 0.5 W, the peak PHC can be calculated using (1) [5].

$$P_{\mathrm{PPHC}} = (E_{\mathrm{br}} / E_{\mathrm{max}})^2 \cdot 0.5\ \mathrm{W} \tag{1}$$

The simulated E_{max} value is 15 KV/m for the 0.5-W input power, and hence, the PPHC is calculated to be 20 KW.

B. APHC

The APHC is limited by the heat defection temperature (HDT) of the building material, i.e., the resin polymer, of the magic-T. The HDT is 268 ℃ for the ceramic-filled resin used in this work. The thermal simulation was performed using CST EM-thermal coupled solvers. The EM solver calculated the microwave loss in the magic-T, and then the generated heat was adopted as a heat source in the thermal solver. In order to make an accurate prediction in the thermal simulation, the electrical conductivity of the copper boundaries for the magic-T was adjusted to fit the re-simulated loss to the measured value, giving a conductor loss of about 0.5 dB for the in-phase input and about 0.3 dB for the out-of-phase input. These values are approximately the maximum losses calculated from the measured result. In the thermal simulation, the magic-T was modeled as it was practically fabricated—a ceramic-filled resin base coated with a layer of 30-μm thick copper. The copper layer was thickened in the fabrication process because the copper thickness had a strong influence on the thermal conductivity of the structure [9]. The thermal conductivity of the ceramic-filled resin was estimated to be 2–14 W/m/K [26]. A moderate thermal conductivity value of 8 W/m/K was used in the thermal simulation. The boundary conditions for the thermal simulation was set so that the bottom face of the magic-T was attached to a thermal sink and the other faces were thermally isolated. The ambient temperature in the thermal simulation was set to be 293 K.

Fig.13(a) shows the thermal-simulated temperature distribution of the magic-T under input power of 100 W at the in-phase input. The maximum simulated temperature is about 266 °C and is close to the HDT of the ceramic-filled resin. On the other hand, as shown in Fig. 13(b), when the same input power is injected from the out-of-phase input, the maximum simulated temperature is only about 40 °C. This is because the out-of-phase transmission loss is lower and less heat would be generated. It should be mentioned that the APHC could be significantly enhanced if printing material with much larger thermal conductivity (e.g. metal) were used, however, for this particular device, as the dimensions of the TL is very small, very fine metal 3D printing machine must be used, such as the one in [31].

Finally, a quantitative comparison in the major features and specifications of the proposed magic-T to previously reported *E*-plane waveguide magic-T demonstrations are summarized in Table IV. First, to the authors' best knowledge, it is the first time that the air-filled self-suspended coaxial TL is applied to the magic-T and resultant magic-T exhibits potentially enhanced power handling capability over the one composed of microstrip probe transition. Compared to the metallic waveguide magic-T in [8], the power handling capability is lower and is limited by the resin-based building material. The power handling capability of the magic-T could be greatly enhanced if better thermally conductive 3-D printing material were used. As can be seen, with the use of 3-D printing technology, the entire magic-T structure can be fabricated as one single part, eliminating the assembly and minimizing the associated tolerance. The good RF performance—transmission losses lower than 0.8 dB; port RLs over 12 dB; isolations greater than 16 dB; absolute amplitude and phase imbalances smaller than 0.5 dB and 3°, respectively—in a relatively broad

operational bandwidth of 42% indicates reasonable structural design and high accuracy of the utilized fabrication process.

VI. Conclusion

Design, implementation, and characterization of a new class of *E*-plane waveguide magic-T based on air-filled rectangular-coax-to-waveguide transitions are presented systematically. The work features enhanced design and fabrication flexibility with the use of polymer-based SLA 3-D printing. Monolithic prototyping of the magic-T is realized, which significantly simplifies the fabrication process, eliminating the assembly tolerance, and dramatically reducing the device weight. The 3-D printed *X*-band magic-T demonstrates port RLs of over 12 dB and isolations higher than 30 dB, with amplitude and phase imbalances of -0.4–0.2 dB and (-3–3)° for in-phase transmission, and -0.5–0 dB and (-1–3)° for out-of-phase transmission, respectively.

Acknowledgment

The authors thank Mr. J. Xiang at Shanghai New East China Institute of Optoelectronic Technology, Shanghai, China, for printing some of the devices.

References

[1] Y. Lou, C. H. Chan, and Q. Xue, "An in-line waveguide-to-microstrip transition using radial-shaped probe," *IEEE Microw. Compon. Lett.*, vol. 18, no. 5, pp. 311–313, May 2008.

[2] F. J. Villegas, D. I. Stones, and H. A. Hung, "A novel waveguide-to-microstrip transition for millimeter-wave module applications," *IEEE Trans. Microw. Theory Techn.*, vol. 47, no. 1, pp. 48‑55, Jan. 1999.

[3] V. S. Möttönen, "Wideband coplanar waveguide-to-rectangular waveguide transition using fin-line taper," *IEEE Microw. Compon. Lett.*, vol. 15, no. 2, pp. 119–121, Feb. 2005.

[4] Q.-X. Chu, Z.-Y. Kang, Q.-S. Wu, and D.-Y. Mo, "An in-phase output *Ka*-band traveling-wave power divider/combiner using double ridge-waveguide couplers," *IEEE Trans. Microw. Theory Techn.*, vol. 61, no. 9, pp. 3247–3253, Sept. 2013.

[5] Q.-X. Chu, Q.-S. Wu, and D.-Y. Mo, "A *Ka*-band *E*-plane waveguide magic-T with coplanar arms," *IEEE Trans. Microw. Theory Techn.*, vol. 62, no. 11, pp. 2673–2679, Nov. 2014.

[6] L. Guo, J. Li, W. Huang, H. Shao, T. Ba, T. Jiang, Y. Jiang, and G. Deng, "A waveguide magic-T with coplanar arms for high-power solid-state power combining," *IEEE Trans. Microw. Theory Techn.*, vol. 65, no. 8, pp. 2942–2952, Aug. 2017.

[7] Y.-J. He, D.-Y. Mo, Q.-S. Wu, and Q.-X. Chu, "A Ka-band waveguide magic-T with coplanar arms using ridge-waveguide transition," *IEEE Microw. Compon. Lett.*, vol. 27, no. 11, pp. 965–967, Nov. 2017.

[8] F. F. He, K. Wu, W. Hong, H. J. Tang, H. B. Zhu, and J. X. Chen, "A planar magic-T using substrate integrated circuits concept," *IEEE Microw. Compon. Lett.*, vol. 18, no. 6, pp. 386–388, Jun. 2008.

[9] F. Zhu, W. Hong, J.-X. Chen, and K. Wu, "Design and implementation of a broadband substrate integrated waveguide magic-T," *IEEE Microw. Compon. Lett.*, vol. 22, no. 12, pp. 630–632, Dec. 2012.

[10] F. F. He, K. Wu, W. Hong, L. Han, and X. Chen, "A planar magic-T structure using substrate integrated circuits concept and its mixer applications," *IEEE Trans. Microw. Theory Techn.*, vol. 59, no. 1, pp. 72‑79, Jan. 2011.

[11] W. Feng, W. Che, and K. Deng, "Compact planar magic-T using E-plane substrate integrated waveguide (SIW) power divider and slotline transition," *IEEE Microw. Compon. Lett.*, vol. 20, no. 6, pp. 331–333, Jun. 2010.

[12] T.-M. Shen, T.-Y. Huang, C.-F. Chen, and R.-B. Wu, "A laminated waveguide magic-T with bandpass filter response in multilayer LTCC," *IEEE Trans. Microw. Theory Techn.*, vol. 59, no. 3, pp. 584‑592, Mar. 2011.

[13] W. Peng, Q. Xiao, and X. Chen, "K-band planar magic-T using LTCC technology," *IEEE Microw. Compon. Lett.*, vol. 27, no. 8, pp. 715–717, Aug. 2017.

[14] Y. Wang, K. Ma, and S. Mou, "A low-loss self-packaged magic-T with compact size using SISL technology," *IEEE Microw. Compon. Lett.*, vol. 28, no. 1, pp. 13–15, Jan. 2018.

[15] J. Li, C. Guo, Y. Yu, G.-L. Huang, T. Yuan, Y. Wang, J. Xu, and A. Zhang, "A full *X*-band fully 3-D printed *E*-plane rectangular-coax-to-waveguide transition," in *IEEE MTT-S Int. Microw. Symp. Dig.*, Boston, MA, Jun. 2019, accepted.

[16] Y. Saito, D. Fontaine, J.-M. Rollin, and D. S. Filipovic, "Monolithic micro-coaxial power dividers," *Electron. Lett.*, vol. 45, no. 9, pp. 469–470, Apr. 2009.

[17] M. J. Lancaster, J. Zhou, M. Ke, Y. Wang, and K. Jiang, "Design and high performance of a micromachined *K*-band rectangular coaxial cable," *IEEE Trans. Microw. Theory Techn.*, vol. 55, no. 7, pp. 1458‑1553, Jul. 2007.

[18] Y. Wang, M. Ke, M. J. Lancaster, and F. Huang, "Micromachined millimeter-wave rectangular-coaxial branch-line coupler with enhanced bandwidth," *IEEE Trans. Microw. Theory Techn.*, vol. 57, no. 7, pp. 1655‑1660, July 2009.

[19] D. M. Pozar, *Microwave Engineering, Third Edition*. New York, NY, USA: John Wiley & Sons, Inc., 2005.

[20] J. R. Reid, E. D. Marsh, and R. T. Webster, "Micromachined rectangular-coaxial transmission lines," *IEEE Trans. Microw. Theory Techn.*, vol. 54, no. 8, pp. 3433‑3442, Aug. 2006.

[21] Y. Wang, X. Shang, and M. J. Lancaster, "Micromachined 3D millimeter-wave and terahertz devices," in *Proc. IEEE MTT-S IMWS-AMP*, Suzhou, China, Jul. 2015, pp. 1–3.

[22] E. D. Marsh, J. R. Reid, and V. S. Vasilyev, "Gold-plated micromachined millimeter-wave resonators based on rectangular coaxial transmission lines," *IEEE Trans. Microw. Theory Techn.*, vol. 55, no. 1, pp. 78‑84, Jan. 2007.

[23] C. Guo, X. Shang, J. Li, F. Zhang, M. J. Lancaster, and J. Xu, "A lightweight 3-D printed *X*-band bandpass filter based on spherical dual-mode resonators," *IEEE Microw. Compon. Lett.*, vol. 26, no. 8, pp. 568–570, Aug. 2016.

[24] X. Shang *et al.*, "W-Band Waveguide Filters Fabricated by Laser Micromachining and 3-D Printing," in *IEEE Transactions on Microwave Theory and Techniques*, vol. 64, no. 8, pp. 2572-2580, Aug. 2016.

[25] J. Li, C. Guo, L. Mao, J. Xiang, G.-L. Huang, and T. Yuan, "Monolithically 3-D printed hemispherical resonator waveguide filters with improved out-of-band rejections," *IEEE Access*, vol. 6, no. 1, pp. 57030–57048, Oct. 2018.

[26] H. Yong and G. Du, "Ceramic/polymer composites with high thermal conductivity and mechanical strength for electronic packaging," in *Proc. Int. Conf. Compos. Mater.*, Xi'an, China, Aug. 2017, pp. 1–4.

[27] M. Salek *et al.*, "W-Band Waveguide Bandpass Filters Fabricated by Micro Laser Sintering," in *IEEE Transactions on Circuits and Systems II: Express Briefs*, vol. 66, no. 1, pp. 61-65, Jan. 2019.

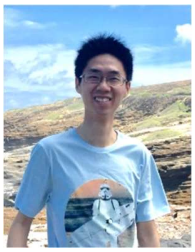

Cheng Guo was born in Chengdu, China, in 1990. He received the B.Eng. degree in communication engineering from Southwest Jiaotong University (Emei), Chengdu, China, in 2012, and the Ph.D. degree in radio physics from University of Electronic Science and Technology of China (UESTC), Chengdu, China, in 2016. From 2014 to 2016, he was a visiting Ph.D. student of the University of Birmingham and a Research Fellow with the same university from 2017-2018. He is now an associate professor with School of information and communications engineering, Xi'an Jiao-tong university. His current research interests include 3-D printed passive microwave devices, Schottky diode-based THz frequency multipliers and mixers, as well as micromachined MMW/THz circuits. He is the recipient of the IEEE-MTTs Tatsuo Itoh Award in 2017.

Jin Li author's bio currently not available

Yang Yu was born in Tianjin, P.R.China, in 1991. He received the B.Eng. degree in communication engineering and the M.Eng. degree in information and communication engineering at Tianjin Polytechnic University, Tianjin, P.R.China, in 2013 and 2016, respectively. He is currently pursuing the Ph.D. degree at University of Birmingham,. He is now a joint Ph.D. student with the University of Birmingham, Birmingham, U.K., and Southern University of Science and Technology, Shenzhen, P.R.China. His recent research focuses on synthesis and design of RF/microwave components and computational intelligence techniques for engineering.

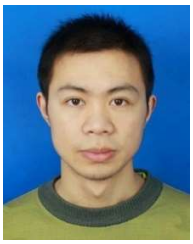

Fan Zhang was born in Sichuan, China. He is currently pursuing the Ph.D. degree in radio physics at School of Physics, University of Electronic Science and Technology of China, Chengdu, China.

From 2017 to 2018, he was a Visiting Student with University of Birmingham, Birmingham, U.K.. His current research interests include design of microwave filters, 3-D printed filters, tunable filters, and millimeter-wave circuits.

Yujian Zhu was born in Zhoukou, China, in 1993. He received the B.E. degree in electronic information engineering from the Anyang Institute of Technology, Anyang, China, in 2016. He is currently pursuing the master's degree in information and communication engineering with Shenzhen University, Shenzhen, China. His current research interests include the patch antennas and waveguide slot antennas.

Qian Yang received the B.S., M.S., and Ph.D. degrees in electromagnetic fields and microwave technology from Xidian University, Xi'an China, in 2007, 2010, and 2017, respectively. From 2010 to 2012, she worked in Shaanxi Huanghe Co., Ltd. She is now a post doctor with School of information and communications engineering, Xi'an Jiao-tong University. Her research interests include antennas and microwave filters design.

Weijun Zhu was born in Linfen, China, in 1983. He received the Ph.D. degree in mechanical engineering from Xi'an Jiaotong University, Xi'an, China, in 2013. From 2011 to 2012, he was a visiting Ph.D. of the Konstanz University, Germany. He is now an associate professor with School of Mechanical Engineering and Automation, Beihang University. His current research interest is the development of hybrid additive manufacturing technologies for devices with multiple functions including mechanics, electromagnetics, thermodynamics, etc.

Shitao Zhu (s'07) received the B.S. degree in electronic Information Science and Technology from Lanzhou University in 2005, Lanzhou, China, and the M.S. degree in Information and Communication Engineering and the Ph.D. degree in electronic science and technology from Xi'an Jiaotong University in 2016, Xi'an, China. He is now a postdoctor in the Department of Information and Communication Engineering, Xi'an Jiaotong University, Xi'an, China. From 2008 to 2012, he was a systems engineer with the ZTE co., LTD, Xi'an, China. His research interests are in the areas of digital predistortion linearization, array signal processing, microwave radar coincidence imaging and metamaterial based microwave device.

Xiaobang Shang (M'13–SM'19) was born in Hubei, China, in 1986. He received the B.E. degree (First Class) in electronic and communication engineering at University of Birmingham, Birmingham, U.K., in 2008, the B.E. degree in electronics and information engineering at Huazhong University of Science and Technology, Wuhan, China, in 2008, and the Ph.D. degree in microwave engineering at the University of Birmingham in 2011. His doctoral research concerned micromachined terahertz circuits and design of multi-band filters. He is currently a Senior Research Scientist with the National Physical Laboratory (NPL), Middlesex, U.K.. Prior to joining the NPL, he was a Research Fellow with the University of Birmingham. His current main research interests include microwave measurements, microwave filters and multiplexers, and micromachining techniques. Dr. Shang was the recipient of the ARFTG Microwave Measurement Student Fellowship Award in 2009, the co-recipient of the IEEE Microwave Theory and Techniques Society Tatsuo Itoh Award in 2017.

Yang Gao received the B.Eng. degree in telecommunication engineering from the Beijing Institute of Technology, Beijing, China, in 2014, and the Ph.D. degree in microwave engineering from the University of Birmingham, Birmingham, U.K., in 2018. After graduating from the University of Birmingham, he joined Zhengzhou University, Zhengzhou, China, as a Lecturer. In 2019, he was employed by the Department of International Cooperation, Ministry of Science and Technology of China on secondment. He is also an Honorary Research Fellow with the Emerging Device Technology Group, University of Birmingham. Yang's current research interests include integrated microwave-terahertz circuits, passive and active components.

Yi Wang (M'09–SM'12) was born in Shandong, China. He received the B.Sc. degree in physics and M.Sc. degree in condensed matter physics at University of Science and Technology, Beijing, China, in 1998 and 2001, respectively, and the Ph.D. degree in electronic and electrical engineering at University of Birmingham, Birmingham, U.K., in 2005.

In 2011, he became a Senior Lecturer and then a Reader at University of Greenwich. In 2018, he joined the University of Birmingham as a Senior Lecturer. His current research interests include millimeter-wave and terahertz devices for metrology, communications and sensors, micromachining, microwave circuits based on multiport filtering networks, and filter-antenna integration.

Guan-Long Huang (M'11-SM'18) received the B.E. degree in electronic information engineering at Harbin Institute of Technology, Harbin, P.R.China, and the Ph.D. degree in electrical and computer engineering at National University of Singapore, Singapore.

He is now with the College of Electronics and Information Engineering, Shenzhen University, Shenzhen, Guangdong, P.R.China. Prior to join the university, he has been with the Temasek Laboratories at National University of Singapore as a Research Scientist, and the Nokia Solutions and Networks System Technology as a Senior Antenna Specialist from 2011 to 2017. His research interests include design and implementation of planar antenna arrays, 5G base-station and mobile RF front-end devices/antennas, phased antenna arrays, and 3-D printing technology in microwave applications. He has authored or co-authored more than 100 papers in journals and conferences. He is now serving as an Associate Editor for the journal IEEE Access.

Qingsha S. Cheng received the B.Eng. and M. Eng. from Chongqing University, China, in 1995 and 1998, respectively. He received his Ph.D. at McMaster University, Canada, in 2004. In 1998, he was with the Department of Computer Science and Technology, Peking University, China. In 2004, he became a postdoctoral fellow and then a research engineer in 2007, both with the Department of Electrical and Computer Engineering, McMaster University. In 2014, he joined Southern University of Science and Technology (SUSTech), Shenzhen, China as an assistant professor in the Department of Electrical and Electronic Engineering. His research interests are surrogate modeling, computer-aided design and tuning, design and modeling of microwave circuits, software design technology, methodologies for microwave CAD and 3D printing technology. He has authored or co-authored more than 100 publications in technical book chapters, refereed international technical journals, refereed international conference proceedings and international workshops. His works have been cited nearly 2500 times according to Google scholar.

Anxue Zhang received his B.S. degree in electrical and electronics engineering from Henan Normal University in 1996 and M.S. and Ph.D. degrees in electromagnetic and microwave engineering from Xi'an Jiaotong University, Xi'an, China, in 1999 and 2003, respectively. He is now a professor at Xi'an Jiaotong University. His main research fields include antenna and electromagnetic wave propagation, RF and microwave circuit design, and metamaterials, with applications to radar and wireless communications.